Journal of Applied Biomechanics, 2006; 22:120-130. © 2006 Human Kinetics, Inc.

Response Surface Optimization for Joint Contact Model Evaluation

Yi-Chung Lin[1], Jack Farr[3], Kevin Carter[4], and Benjamin J. Fregly[1,2]

[1,2]University of Florida; [3]Cartilage Restoration Center of Indiana; [4]Regeneration Technologies, Inc.

When optimization is used to evaluate a joint contact model's ability to reproduce experimental measurements, the high computational cost of repeated contact analysis can be a limiting factor. This paper presents a computationally-efficient response surface optimization methodology to address this limitation. Quadratic response surfaces were fit to contact quantities (contact force, maximum pressure, average pressure, and contact area) predicted by a discrete element contact model of the tibiofemoral joint for various combinations of material modulus and relative bone pose (i.e., position and orientation). The response surfaces were then used as surrogates for costly contact analyses in optimizations that minimized differences between measured and predicted contact quantities. The methodology was evaluated theoretically using six sets of synthetic (i.e., computer-generated) contact data, and practically using one set of experimental contact data. For the synthetic cases, the response surface optimizations recovered all contact quantities to within 3.4% error. For the experimental case, they matched all contact quantities to within 6.3% error except for maximum contact pressure, which was in error by up to 50%. Response surface optimization provides rapid evaluation of joint contact models within a limited range of relative bone poses and can help identify potential weaknesses in contact model formulation and/or experimental data quality.

[1]Mechanical & Aerospace Engineering, 231 MAE-A Bldg., and [2]Biomedical Engineering, University of Florida, Gainesville, FL 32611; [3]Cartilage Restoration Center of Indiana, 1550 E. County Line Rd, Suite 200, Indianapolis, IN 46227; [4]Regeneration Technologies Inc., 11621 Research Circle, Alachua, FL 32615.

Key Words: surrogate-based modeling, contact analysis, knee mechanics

Knowledge of in vivo contact forces and pressures in human joints would be valuable for preventing and treating joint injuries and for improving the longevity of joint replacements. Unfortunately, contact conditions are difficult to measure in vivo (Kaufman, Kovacevic, Irby, & Colwell, 1996), necessitating model-based analyses to develop predictions as well as static in vitro testing to evaluate these predictions. A variety of joint contact modeling methods have been used for this purpose, including finite element (Bendjaballah, Shirazi-Adl, & Zukor, 1998; Donahue, Rashid, Jacobs, & Hull, 2002; Stolk, Verdonschot, Cristofolini, Toni, & Huiskes, 2002), boundary element (Haider & Guilak, 2000; Kuo & Keer, 1993), and discrete element methods (Dhaher & Kahn, 2002; Li, Lopez, & Rubash, 2001; Piazza & Delp, 2001).

Once a joint contact model has been created that represents an in vitro testing situation, its ability to reproduce experimentally measured contact quantities must be evaluated. At least two factors can complicate this process. The first is uncertainties in the experimental measurements. These uncertainties can often be estimated and involve quantities such as the pose of cadaveric bones measured during testing, contact pressures and areas recorded by a pressure sensor, the articular surface geometry determined from medical imaging data, and material parameters in the contact model.

A second complicating factor is the high computational cost of repeated contact analysis. Given an estimated envelope of uncertainty, optimization

methods can be used to determine whether a feasible combination of model parameters could be used to reproduce all experimental measurements simultaneously (Fregly, Bei, & Sylvester, 2003). The problem with this approach is that the high computational cost of repeated contact analysis can make such optimizations extremely time consuming and in some cases even impractical.

Response surface methods have been utilized successfully in other domains to eliminate computational bottlenecks in optimization studies. Response surfaces are multidimensional surface fits to quantities of interest (i.e., responses) predicted by an engineering model. Once the mathematical form of a response surface is specified, linear least squares is typically used to determine the coefficients that provide the best fit to each response as a function of the specified design variables. These surface approximations are then used as surrogates for costly engineering analyses when the optimization is performed. To our knowledge, no published studies have used response surface methods to perform optimizations of contact problems.

This paper presents a computationally efficient response surface methodology for performing fast optimizations involving joint contact models. The theoretical soundness of the approach is demonstrated by reproducing six sets of synthetic contact data generated by a discrete element contact model of the tibiofemoral joint. The practical applicability is assessed by attempting to match static experimental contact data collected from the same cadaveric specimen used to create the joint contact model. The results demonstrate not only the soundness and computational efficiency of the proposed approach but also its ability to identify potential weaknesses in contact model formulation and/or quality of available experimental data.

Methods

Response Surface Approximations

The response surface method can be defined as a collection of statistical and mathematical techniques useful for constructing smooth approximations to functions in a multidimensional design space. Once a mathematical form has been selected, the coefficients of the approximating function (response surface) are determined using data from either physical experiments or numerical simulations. The most common mathematical form for a response surface is a quadratic polynomial. For two design variable inputs x_1 and x_2 and output variable y, a quadratic response surface would take the form

$$y = \beta_0 + \beta_1 x_1 + \beta_2 x_2 + \beta_3 x_1^2 + \beta_4 x_2^2 + \beta_5 x_1 x_2 \quad (1)$$

where the β_i ($i = 0,\ldots,5$) are the unknown coefficients to be fitted from an overdetermined data set. Response surface approximations work best when the number of design variable inputs is small (< 10), since a large number of design variables results in a complicated design space that is difficult to fit with low-degree polynomials or other analytical functions.

To develop response surface approximations for contact problems, one must identify the design variable inputs, the outputs to be predicted, and the mathematical form of the response surface relating them. For a linear elastic contact model evaluated using static experimental data, the design variables are the six relative pose parameters (3 translations and 3 rotations) and material modulus of the contacting bodies. The response surface outputs are contact force, maximum pressure, average pressure, and contact area. These quantities can be calculated by the contact model and measured experimentally for comparison. The hypothesized mathematical form is a quadratic response surface with one modification. For a linear elastic contact model, the material modulus (assumed to be the same for both bodies) linearly scales each contact quantity except area (Johnson, 1985). Thus, data for the response surfaces are generated using a material modulus of one, the six pose parameters are used as the response surface inputs, and the response surface outputs (except area) are scaled by the desired modulus value.

With the response surface formulation specified, the next step is to determine a sampling scheme within the design space to provide data for fitting the response surface. Since this sampling process is only performed once to generate the response surfaces, the computational cost of repeated contact analysis is paid only once up front. Though a 6-dimensional quadratic response surface requires only 28 sample points to solve for all unknown coefficients, we use an overdetermined set of 77 sample points for consistency with a 6-dimensional face-

centered central composite sampling scheme. To cover the design space as uniformly as possible, we choose these points using Latin hypercube sampling, which places only one sample point in each row and column of the 6-dimensional design space.

For contact analyses, we make two modifications to the Latin hypercube sampling scheme to improve the quality of the fit. The first modification accounts for infeasible points. A sampled point is deemed to be infeasible and is therefore omitted if the contact force and area predicted by the contact model are zero. This modification avoids fitting regions of the design space where no contact is occurring. The second modification accounts for outlier points. Once a response surface is generated from feasible points, the output is compared to the computed value from the contact model for every sample point. The point with the largest absolute percent error above a preselected cutoff value of 10% (a typical value for engineering analyses) is omitted and the response surface is regenerated from the remaining sample points. The procedure is iterated until all sample points are below 10% error. This modification provides the best fit in the regions of interest where the contact force is large.

After a response surface is generated, the quality of the resulting fit must be assessed, since a poor quality fit indicates that a different mathematical form for the response surface should be considered. We use three common error measures for this purpose. The first measure of fit quality is the adjusted root mean square error ($RMSE_{adj}$). Unlike the standard RMSE, the adjusted version uses $n - p$ rather than n in the denominator:

$$RMSE_{adj} = \sqrt{\frac{\sum_{i=1}^{n}(y_i - \hat{y}_i)^2}{n-p}} \tag{2}$$

where n is the number of sample points ($n > 28$ and $n \leq 77$), p is the number of fitting parameters ($p = 28$), y_i are the actual responses computed by the contact model, and $\hat{y}_i$ are the responses predicted from the response surface. To provide a relative measure of fit quality, we also compute the percent adjusted *RMSE* using

$$\%RMSE_{adj} = \frac{100}{\tilde{y}}\sqrt{\frac{\sum_{i=1}^{n}(y_i - \hat{y}_i)^2}{n-p}} \tag{3}$$

where $\tilde{y}$ represents the average magnitude of the fitted quantity:

$$\tilde{y} = \frac{1}{n}\sum_{i=1}^{n}|y_i| \tag{4}$$

The second measure of fit quality is the adjusted coefficient of determination (R^2_{adj}). Similar to the adjusted RMSE, the adjusted R^2 value uses $n - p$ to account for the degrees of freedom remaining in the fit:

$$R^2_{adj} = 1 - \frac{\sum_{i=1}^{n}(y_i - \hat{y}_i)^2/(n-p)}{\sum_{i=1}^{n}(y_i - \bar{y})^2/(n-1)} \tag{5}$$

where $\bar{y}$ is the mean of the actual responses.

The final measure of fit quality is the *RMSE* calculated from the prediction error sum of squares (*PRESS*) statistic. To evaluate the predictive capability of a response surface, the *PRESS* analysis excludes one sample point at a time from the set used to generate each response surface. The response surface is regenerated using the remaining $n - 1$ sample points and the prediction error (called the *PRESS* residual) at the omitted sample point is calculated. This process is repeated for all n sample points, and the resulting sum of squares of *PRESS* residuals is called the *PRESS* statistic. Finally, a *PRESS*-based *RMSE* is calculated as

$$RMSE_{PRESS} = \sqrt{\frac{PRESS\ statistic}{n}} \tag{6}$$

Once accurate response surfaces are generated for the output quantities of interest, they are used in an optimization to evaluate the contact model's ability to reproduce experimental measurements. Each time the optimization requires contact quantities from the contact model, a response surface is used in place of a contact analysis to provide the values. By fitting multiple outputs of the contact model, one can create any cost function that can be built up from response surface outputs without the need for additional contact analyses.

Discrete Element Contact Model

A discrete element contact model of the tibiofemoral joint was constructed to evaluate the proposed response surface methodology. Details of the model creation process can be found in Bei and Fregly (2004). In brief, MRI and CT data were

collected from a single cadaveric knee specimen cut approximately 15 cm above and below the joint line and showing no visible signs of degenerative joint disease. Three titanium bone screws were inserted into the tibia and femur as landmarks for contact model alignment. The tibia, femur, and bone screws were segmented using commercial image processing software (SliceOmatic, Tomovision, Montreal, Canada). For simplicity, the menisci were not segmented and were omitted from the model. The resulting point clouds from both scans were exported, aligned, and merged for surface creation using commercial reverse engineering software (Geomagic Studio, Raindrop Geomagic, Research Triangle Park, NC) (Figure 1a). The final composite geometric model possessed articular cartilage surfaces from MRI and cortical bone and bone screw surfaces from CT (Figure 1b).

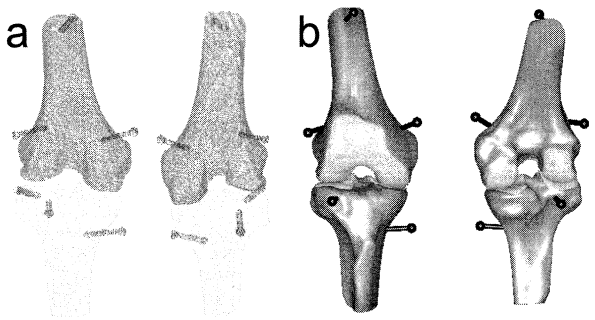

Figure 1 – Anterior and posterior views of discrete element contact model of the tibiofemoral joint. (a) 3D point clouds; (b) Resulting 3D NURBS surfaces. Surface geometry for articular cartilage, subchondral bone, and bone screws was obtained from CT and MR images.

The geometric surfaces for the tibia and femur (articular cartilage, cortical bone, and bone screws) were imported into Pro/Mechanica Motion (Parametric Technology Corp., Waltham, MA) to construct a multibody contact model. The mean digitized bone screw locations from static contact experiments described below were also imported to determine a nominal alignment of the tibia and femur. For both bones, a stiff linear spring was placed between each bone-fixed screw head and its corresponding lab-fixed digitized location, and a static analysis was then performed to find the static pose that best matched the experiments. Differences between the digitized and modeled bone screw locations were on the order of 1 mm. Starting from this nominal pose, the tibia was fixed to ground and the femur was connected to the tibia via a 6 degree-of-freedom (DOF) joint.

Custom contact code was incorporated into the multibody model and was used to solve for the medial and lateral contact conditions as a function of the 6 DOFs between the two bones (Bei & Fregly, 2004). The contact code implemented a linear elastic discrete element contact model, where the pressure p for each contact element on the tibial articular surfaces (An, Himeno, Tsumura, Kawai, & Chao, 1990; Blankevoort, Kuiper, Huiskes, & Grootenboer, 1991; Li, Sakamoto, & Chao, 1997) was calculated from

$$p = \frac{(1-\nu)E}{(1+\nu)(1-2\nu)}\frac{d}{h} \tag{7}$$

where E is Young's modulus of the articular cartilage, ν is Poisson's ratio, h is the combined thickness of the femoral and tibial articular cartilage, and d is the interpenetration of the undeformed contact surfaces. Both h and d were calculated using the ACIS 3D Toolkit (Spatial Corp., Westminster, CO). Poisson's ratio was set to 0.45 (Blankevoort et al., 1991) and Young's modulus was set to 1 MPa to facilitate its use as a design variable in the subsequent response surface optimizations.

Synthetic and Experimental Contact Data

To demonstrate the theoretical soundness and practical applicability of the proposed response surface optimization approach, we performed repeated response surface optimizations using synthetic and experimental contact data. Synthetic contact data were generated by placing the discrete element knee model in six configurations consistent with all possible combinations of three flexion angles (0°, 45°, and 90°) and two vertically applied loads (500 N and 1000 N). Young's modulus was set to be the value obtained from response surface optimization of the experimental contact data (2.5 MPa).

The experimental contact data were obtained from the same cadaveric specimen used for contact model creation. Prior to contact pressure testing, the menisci, fibula, and patella were removed. The specimen was mounted in an MTS MiniBionix 858 servohydraulic test machine at a flexion angle of

Figure 2 – Overview of experimental setup. A human cadaveric knee specimen was mounted in an MTS servohydraulic test machine with a fixed flexion angle of 30°. An axial load of 1000 N was applied to the specimen, and intraarticular contact force, pressure, and area were measured in the medial and lateral compartments using a Tekscan K-Scan sensor. A Microscribe 3DX digitizer was used to record the location of three titanium bone screws mounted in the tibia and femur at the final static pose.

30° (Figure 2). A Tekscan K-scan sensor (Tekscan, South Boston, MA) was inserted anteriorly into the medial and lateral joint space. The specimen was then subjected to three trials of a 4-second ramp load from 200 to 1000 N (Alhalki, Hull, & Howell, 2000). At the end of each ramp, we measured four experimental quantities of interest from the medial and lateral compartments: contact force, maximum pressure, average pressure, and contact area. In addition, the locations of the six screw heads were digitized using a Microscribe 3DX digitizer (Immersion Corp., San Jose, CA) possessing an accuracy of 0.23 mm. The resulting data points from the K-scan sensor and digitizer were averaged over the three trials and used for practical evaluation of the response surface optimization methodology.

Response Surface Evaluation

The response surface methodology was evaluated using three approaches. First, the statistical measures described above were used to evaluate the ability of each response surface to reproduce the sample points generated by the discrete element contact model. Eight responses surfaces (medial and lateral contact force, maximum pressure, average pressure, and contact area) were created for each of the seven data sets (six synthetic and one experimental). For each data set, pose variations for the 77 Latin hypercube sample points were defined to be within ±1 mm and ±1° from the nominal pose based on the estimated envelope of experimental pose uncertainty.

Second, the sensitivity of the eight contact quantities to pose variations of ±1 mm and ±1° away from the nominal experimental pose was calculated to evaluate the reasonableness of using quadratic response surfaces. For each data set, the shape of each sensitivity curve provided two important pieces of information: whether a quadratic response surface is an appropriate analytical model, and whether the variations in contact quantities with small pose variations are large enough to warrant the use of the response surface methodology. All sensitivity curves were generated using a Young's modulus

value of 2.5 MPa, consistent with the experimental contact data.

Third, optimizations were performed to evaluate the accuracy and speed with which the response surfaces could recover known or measured contact quantities. For each data set, 1000 nonlinear least-squares optimizations were performed with the Matlab Optimization Toolbox (The Mathworks, Natick, MA) to seek the global optimum. The cost function $g(\mathbf{x})$ minimized percent errors in synthetic or experimental average (p_{ave}) and maximum (p_{max}) pressures in both compartments simultaneously with a penalty term on contact force (F) errors:

(*see Eq 8 below*)

where $\hat{p}_{ave}(\mathbf{x})$, $\hat{p}_{max}(\mathbf{x})$, and $\hat{F}(\mathbf{x})$ are the average pressure (MPa), maximum pressure (MPa), and contact force (N) predicted by a response surface. In this equation, $\mathbf{x}$ represents the six pose parameter design variables, E is the material modulus design variable, and $w = 10^9$ is the weight of the penalty term. This cost function mimics the results of a static analysis, since contact forces are matched closely while relative errors in other cost function terms are minimized. Uniformly distributed random initial guesses were selected within the bounds ±1 for the first six design variables and 1 to 10 for the seventh. A final discrete element contact analysis was performed using the optimized design variables from the best solution to assess the accuracy of the final result.

Results

Quadratic response surfaces fit the eight contact quantities extremely accurately for each set of 77 sample points. On average, for the seven sets of response surfaces, $\%RMSE_{adj}$ was less than 2.2, $\%RMSE_{press}$ was less than 3.0, and R^2_{adj} was greater than 0.997 (Table 1), with corresponding worst-case results of 3.4, 5.8, and 0.993, respectively. For each response surface, a minimum of 0 and maximum of 23 infeasible/outlier points were eliminated from the 77 sample points.

Sensitivity curves for the eight contact quantities as a function of pose parameter changes demonstrated linear or approximately quadratic trends, with the results varying with pose parameter and side (Figure 3). For all seven data sets, contact quantities were highly sensitive to changes in superior-inferior translation, moderately sensitive to changes in varus-valgus rotation, and relatively insensitive to changes in all other pose parameters.

$$
\begin{aligned}
g(\mathbf{x},E) = {} & \left(\left(p_{ave} - E\hat{p}_{ave}(\mathbf{x})\right)/p_{ave}\right)^2_{medial} + \left(\left(p_{ave} - E\hat{p}_{ave}(\mathbf{x})\right)/p_{ave}\right)^2_{lateral} + \\
& \left(\left(p_{\max} - E\hat{p}_{\max}(\mathbf{x})\right)/p_{\max}\right)^2_{medial} + \left(\left(p_{\max} - E\hat{p}_{\max}(\mathbf{x})\right)/p_{\max}\right)^2_{lateral} + \\
& w\left[\left(\left(F - E\hat{F}(\mathbf{x})\right)/F\right)^2_{medial} + \left(\left(F - E\hat{F}(\mathbf{x})\right)/F\right)^2_{lateral}\right]
\end{aligned}
\tag{8}
$$

Table 1 Statistical Measures ($M \pm SD$) of Response Surface Accuracy From the 77 Latin Hypercube Sample Points

Predicted quantity	Side	$\%RMSE_{adj}$	$\%RMSE_{press}$	R^2_{adj}
Force	Medial	0.85 ± 0.37	1.29 ± 0.63	1.000 ± 0.000
Max pressure		1.11 ± 1.11	1.72 ± 2.02	0.999 ± 0.003
Avg pressure		1.90 ± 0.97	2.57 ± 1.27	0.998 ± 0.002
Area		2.10 ± 0.93	2.93 ± 1.21	0.997 ± 0.002
Force	Lateral	0.56 ± 0.36	0.81 ± 0.51	1.000 ± 0.000
Max pressure		0.57 ± 0.15	0.80 ± 0.24	1.000 ± 0.000
Avg pressure		0.67 ± 0.52	0.96 ± 0.75	0.999 ± 0.001
Area		0.73 ± 0.43	1.02 ± 0.64	0.999 ± 0.001

Note: Results indicate mean ± standard deviation as calculated from the 7 data sets (6 synthetic and 1 experimental).

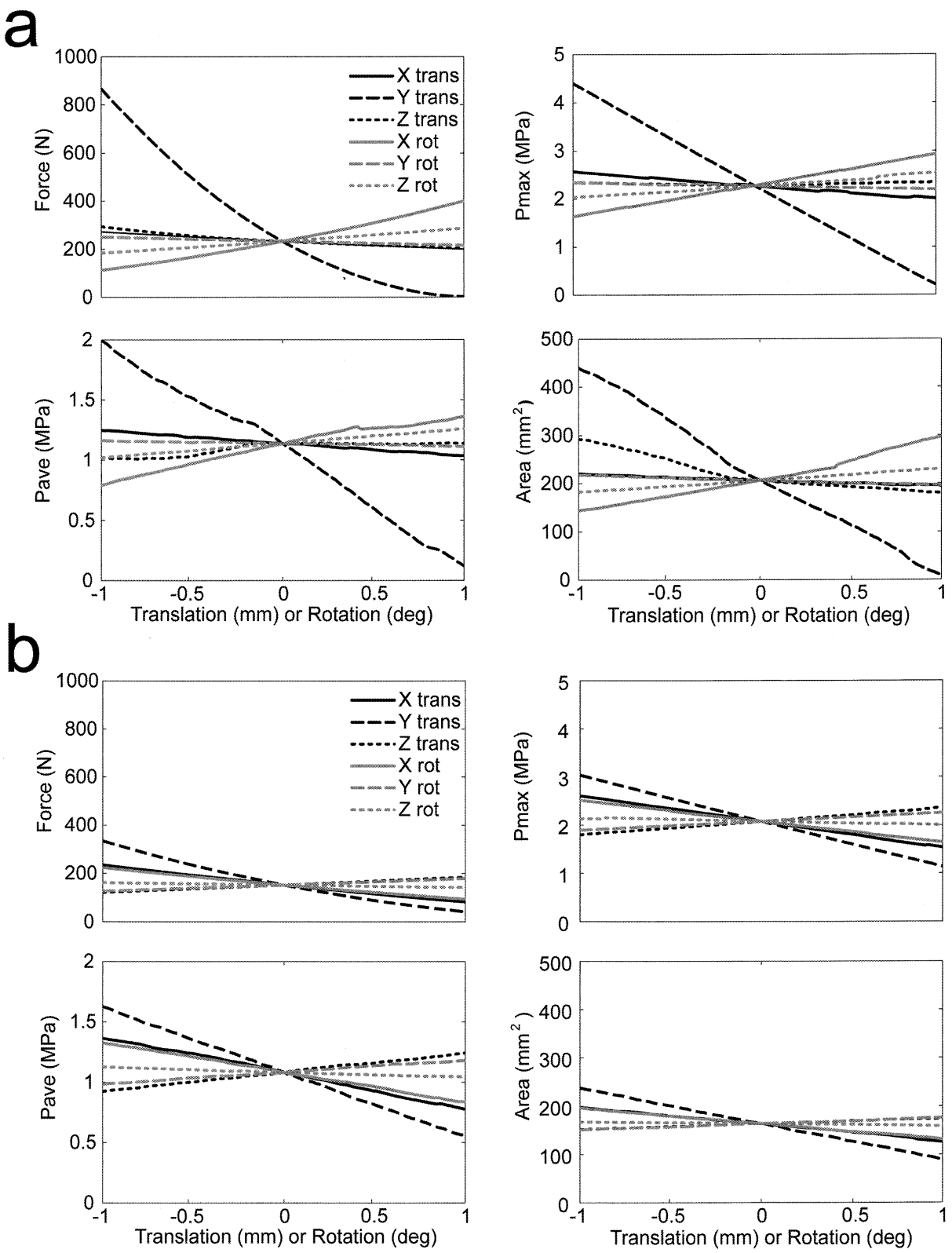

Figure 3 – Sensitivity of predicted contact force (Force), maximum pressure (Pmax), average pressure (Pave), and contact area (Area) to pose parameter variations of ±1 mm and 1° about the nominal experimental pose. (a) Medial side; (b) Lateral side. X is the anterior-posterior direction, Y the superior-inferior direction, and Z the medial-lateral direction.

In addition, medial contact quantities were more sensitive to pose parameter changes than were lateral contact quantities.

The best solution found from each set of 1000 response surface optimizations matched the synthetic or experimental contact quantities extremely well. For the six synthetic data sets, the response surface optimizations recovered the known values of all contact quantities with an average error of less than 1.0% and maximum error of 3.3%, with contact force being recovered with zero error to three decimal places (Table 2). Young's modulus was recovered with an average error of 2.6% and maximum error of 7.7%. While errors as large as 39.6% (internal-external rotation) were observed in the final pose parameters, the two most sensitive pose parameters (superior-inferior translation and varus-valgus rotation) exhibited errors of at most 2.63% and 4.43%, respectively.

When a final contact analysis was performed with the discrete element contact model at the best solution found, average errors in all contact quantities were below 1.3% with a maximum error of 2.8%, consistent with the response surface fitting errors (Table 2). For the experimental data set, the response surface optimizations matched all medial and lateral contact quantities to within 6.3% error with the exception of maximum contact pressure, which was in error by as much as 50% (Table 2). The optimal value of Young's modulus was found to be 2.5 MPa. For each data set, 1000 response surface optimizations required approximately 5 minutes of CPU time on a 2.8 GHz Pentium 4 PC, with the best solution never reaching the bounds of the design variables.

Discussion

This paper has presented a novel response surface optimization methodology that eliminates the computational limitations of performing repeated contact analyses when evaluating a contact model's ability to reproduce experimental data. The theoretical soundness of the methodology was demonstrated by using response surface optimization to recover six sets of synthetic contact data generated by a discrete element model of the tibiofemoral joint. Recovered pose parameter values were the most accurate for the parameters to which the contact quantities were the most sensitive. The practical applicability was shown by using response surface optimization to evaluate the discrete element model's ability to reproduce static experimental contact data collected from the same cadaveric specimen used to construct the model.

The optimized value of Young's modulus (2.5 MPa) was within the range of values reported in the literature for short-term loading (0.4 to 26.8 MPa; Hori & Mockros, 1976; Nieminen et al., 2004; Popko, Mnich, Wasilewski, & Latosiewicz, 1986; Setton, Elliot, & Mow, 1999; Shephard & Seedhom, 1997). By replacing computationally costly contact

Table 2 Percent Errors in Contact Quantities From Response Surface and Discrete Element Models at the Best Solution Found From 1000 Optimizations

Contact quantity	Side	Synthetic Data		Experimental Data	
		Response surface	Discrete element	Response surface	Discrete element
Force	Medial	0.00 ± 0.00	–0.02 ± 1.17	0.00	–0.03
Max pressure		0.16 ± 0.62	0.60 ± 1.11	–49.5	–50.0
Avg pressure		–0.98 ± 1.33	–0.31 ± 1.60	–4.13	–2.86
Area		0.55 ± 1.50	0.30 ± 1.25	4.93	2.75
Force	Lateral	0.00 ± 0.00	–0.05 ± 0.39	0.00	–0.28
Max pressure		0.00 ± 0.77	0.03 ± 0.92	15.4	16.2
Avg pressure		–0.57 ± 1.17	–0.68 ± 1.38	5.48	6.24
Area		0.66 ± 1.56	1.27 ± 0.97	–4.96	–5.77

Note: Synthetic data results indicate mean ± standard deviation errors from the 6 synthetic data sets.

analyses with quadratic RS approximations, optimizations that vary the relative pose of the contacting bodies can be performed rapidly to minimize differences between predicted and measured contact quantities.

Use of response surfaces to replace repeated contact analyses in optimization studies is worthwhile for several reasons. First, response surface tends to smooth out noise in the design space, thereby reducing the risk of entrapment in a local minimum during optimization.

Second, response surface approximations are computationally efficient. Rather then repeating costly contact analyses during an optimization, a single set of costly contact analyses is performed once up front to generate the necessary sample points for response surface approximation. Extremely fast function evaluations allow one to search for the global optimum using either repeated gradient-based optimizations or global optimization.

Third, response surface optimizations are convenient to implement. Optimized contact solutions can be founded utilizing any commercially available optimization algorithm once the response surface approximations are constructed.

Fourth, a variety of optimization problem formulations can be evaluated quickly. Each contact quantity that could potentially appear in the cost function or constraints can be fitted with its own response surface. Different cost functions can then be constructed by weighting contributions from the different response surfaces.

While the computational benefits of the response surface methodology are significant for a discrete element joint contact model, they would be even more significant for a boundary element or finite element joint contact model. On average, 77 discrete element contact analyses to generate sample points required approximately 23 minutes of CPU time on a 2.8 GHz Pentium 4 PC, which is not computationally burdensome. However, 77 static analyses performed with a boundary element or finite element contact model would be expected to take significantly longer. The higher up-front cost to generate response surfaces would be recovered quickly when performing optimizations. Since the use of response surfaces in place of the discrete element contact model reduced optimization time by a factor of 20,000, even larger computational benefits would be expected if response surfaces were used in place of boundary element or finite element joint contact models.

Our results highlight at least three experimental inaccuracies that may have contributed to large maximum pressure errors. First, insertion of a relatively stiff sensor into the joint space may have affected maximum pressure measurements as a function of conformity (Wu, Herzog, & Epstein, 1998). Fifty percent underprediction of maximum pressure on the moderately conformal medial side and 15% overprediction on the nonconformal lateral side are consistent with the conformity trends reported by Wu et al. (1998), where maximum pressure errors were estimated to be between 10 and 26%.

Second, nonuniform response of the sensels on the Tekscan sensor may have caused the measured maximum pressures to be inaccurate. However, the use of a weighted average to calculate maximum pressure would attenuate this effect.

Third, small errors in articular surface geometry may have resulted in large errors in predicted maximum pressures. During MR imaging, the articular cartilage was mildly deformed due to ligamentous forces, resulting in articular surface geometry in the model that did not represent the undeformed state. Furthermore, the MR imaging sequence possessed an in-plane resolution of only 0.3 mm. This value is large considering the sensitivity of maximum contact pressures to changes in superior-inferior translation, especially on the medial side where the largest error occurred (Figure 3). Unfortunately, there is no simple way to modify general surface geometry in a parametric fashion to investigate the influence of small surface geometry changes on maximum pressure errors.

Our results also highlight at least three possible contact model inadequacies. First, the lack of coupling between the contact elements may have affected the predicted maximum pressures. However, due to the thinness of the elastic cartilage layers, the resulting errors would likely be small.

Second, inhomogeneous material properties may have contributed to errors in predicted maximum pressures. Though homogeneous cartilage material models have been used frequently in published studies (Blankevoort et al., 1991; Haut, Hull, Rashid, & Jacobs, 2002; Périé & Hobatho, 1998), recent studies have reported significant local variations in Young's modulus and Poisson's ratio (Hasler, Herzog, Wu, Müller, & Wyss, 1999;

Jurvelin, Arokoski, Hunziker, & Helminen, 2000; Laasanen et al., 2003). Mukherjee and Wayne (1998) reported that articular cartilage regions with the highest Young's modulus correspond to regions with the highest contact pressure and cartilage thickness. This observation is consistent with our results, where an increase in Young's modulus on the medial side (i.e., side with highest in vivo contact pressures) would reduce maximum pressure error.

Third, the omission of time-dependent fluid flow effects may have affected the predicted maximum pressures. However, for loading over a short time period, an elastic contact model may still provide a reasonable approximation of the in vivo situation depending on the intended application of the model (Donzelli, Spilker, Ateshian, & Mow, 1999; Mow, Lai, & Holmes, 1982; Shepherd & Seedhom, 1997).

The main limitation of the proposed response surface methodology is that it has only been evaluated for relatively small variations in pose parameters. Other surrogate modeling methods such as Kriging, support vector machines, or multidimensional spline fitting may be required to cover the full range of pose variations that a particular anatomic joint may experience in vivo. For example, Lin et al. (Lin, Fregley, Haftka, & Queipo, 2005) recently developed a novel spline fitting approach to model the relationship between sagittal joint pose and the net contact forces and torque exerted by the femoral component on the tibial insert of an artificial knee. When used in a planar multibody dynamic simulation, the spline-based surrogate contact models reduced computation time from 28 minutes to less than 90 seconds. Further research is required to extend surrogate contact modeling methods to large 6-DOF pose variations.

Acknowledgments

This study was supported by NIH National Library of Medicine grant R03 LM07332 to B.J. Fregly, and by Regeneration Technologies, Inc. We thank Dr. Raphael Haftka for valuable comments on the use of response surface methods to fit quantities predicted by a joint contact model.

References

Alhalki, M.M., Hull, M.L., & Howell, S.M. (2000). Contact mechanics of the medial tibial plateau after implantation of a medial meniscal allograft. A human cadaveric study. *American Journal of Sports Medicine*, **28**, 370-376.

An, K.N., Himeno, H., Tsumura, H., Kawai, T., & Chao, E.Y.S. (1990). Pressure distribution on articular surfaces: Application to joint stability evaluation. *Journal of Biomechanics*, **23**, 1013-1020.

Bei, Y., & Fregly, B.J. (2004). Multibody dynamic simulation of knee contact mechanics. *Medical Engineering & Physics*, **26**, 777-789.

Bendjaballah, M.Z., Shirazi-Adl, A., & Zukor, D.J. (1998). Biomechanical response of the passive human knee joint under anterior-posterior forces. *Clinical Biomechanics*, **13**, 625-633.

Blankevoort, L., Kuiper, J.H., Huiskes, R., & Grootenboer, H.J. (1991). Articular contact in a three-dimensional model of the knee. *Journal of Biomechanics*, **24**, 1019-1031.

Dhaher, Y.Y., & Kahn, L.E. (2002). The effect of vastus medialis forces on patello-femoral contact: A model-based study. *Journal of Biomechanical Engineering*, **124**, 758-767.

Donahue, T.L.H., Rashid, M.M., Jacobs, C.R., & Hull, M.L. (2002). A finite element model of the human knee joint for the study of tibio-femoral contact. *Journal of Biomechanical Engineering*, **124**, 273-280.

Donzelli, P.S., Spilker, R.L., Ateshian, G.A., & Mow, V.C. (1999). Contact analysis of biphasic transversely isotropic cartilage layers and correlations with tissue failure. *Journal of Biomechanics*, **32**, 1037-1047.

Fregly, B.J., Bei, Y., & Sylvester, M.E. (2003). Experimental evaluation of a multibody dynamic model to predict contact pressures in knee replacements. *Journal of Biomechanics*, **36**, 1658-1668.

Haider, M.A., & Guilak, F. (2000). Axisymmetric boundary integral model for incompressible linear viscoelasticity: Application to the micropipette aspiration contact problem. *Journal of Biomechanical Engineering*, **122**, 236-244.

Hasler, E.M., Herzog, W., Wu, J.Z., Müller, W., & Wyss, U. (1999). Articular cartilage biomechanics: Theoretical models, material properties, and biosynthetic response. *Critical Reviews in Biomedical Engineering*, **27**, 415-488.

Haut, T.L., Hull, M.L., Rashid, M.M., & Jacobs, C.R. (2002). A finite element model of the human knee joint for the study of tibio-femoral contact. *Journal of Biomechanical Engineering*, **124**, 273-280.

Hori, R.Y., & Mockros, L.F. (1976). Indentation tests of human articular cartilage. *Journal of Biomechanics*, **9**, 259-268.

Johnson, K.L. (1985). *Contact mechanics*. Cambridge: Cambridge University Press.

Jurvelin, J.S., Arokoski, J.P., Hunziker, E.B., & Helminen, H.J. (2000). Topographical variation of the elastic properties of articular cartilage in canine knee. *Journal of Biomechanics*, **33**, 669-675.

Kaufman, K.R., Kovacevic, N., Irby, S.E., & Colwell, C.W. (1996). Instrumented implant for measuring tibiofemoral forces. *Journal of Biomechanics*, **29**, 667-671.

Kuo, C.H., & Keer, L.M. (1993). Contact stress and fracture analysis of articular cartilage. *Biomedical Engineering Applications Basis Communications*, **5**, 515-521.

Laasanen, M.S., Toyras, J., Korhonen, R.K., Rieppo, J., Saarakkala, S., Nieminen, M.T., Hirvonen, J., & Jurvelin, J.S. (2003). Biomechanical properties of knee articular cartilage. *Biorheology*, **40**, 133-140.

Li, G., Lopez, O., & Rubash, H. (2001). Variability of a 3D finite element model constructed using MR images of a knee for joint contact stress analysis. *Journal of Biomechanical Engineering*, **123**, 341-346.

Li, G., Sakamoto, M., & Chao, E.Y.S. (1997). A comparison of different methods in predicting static pressure distribution in articulating joints. *Journal of Biomechanics*, **30**, 635-638.

Lin, Y-C., Fregly, B.J., Haftka, R.T., & Queipo,.N.V. (2005). Surrogate-based contact modeling for efficient dynamic simulation with deformable anatomic joints. In *Proceedings of the Tenth International Symposium on Computer Simulation in Biomechanics* (pp. 23-24), Cleveland, OH.

Mow, V.C., Lai, W.M., & Holmes, M.H. (1982). Advanced theoretical and experimental techniques in cartilage research. In R. Huiskes, D. van Campen, & J. DeVijn (Eds.), *Biomechanics: Principles and applications* (pp. 63-69). Boston: Martinus Nijhoff Publ.

Mukherjee, N., & Wayne, J.S. (1998). Load sharing between solid and fluid phases in articular cartilage: I—Experimental determination of in situ mechanical conditions in a porcine knee. *Journal of Biomechanical Engineering*, **120**, 614–619.

Nieminen, M.T., Toyras, J., Laasanen, M.S., Silvennoinen, J., Helminen, H.J., & Jurvelin, J.S. (2004). Prediction of biomechanical properties of articular cartilage with quantitative magnetic resonance imaging. *Journal of Biomechanics*, **37**, 321-328.

Périé, D., & Hobatho, M.C. (1998). In vivo determination of contact areas and pressure of the femorotibial joint using non-linear finite element analysis. *Clinical Biomechanics*, **13**, 394-402.

Piazza, S.J., & Delp, S.L. (2001). Three-dimensional dynamic simulation of total knee replacement motion during a step-up task. *Journal of Biomechanical Engineering*, **123**, 599-606.

Popko, J., Mnich Z., Wasilewski, A., & Latosiewicz, R. (1986). Topographic differences in the value of the 2-sec elastic modulus in the cartilage tissue of the knee joint. *Beitrage zur Orthopadie und Traumatologie*, **33**, 506-509.

Setton, L.A., Elliot, D.M., & Mow, V.C. (1999). Altered mechanics of cartilage with osteoarthritis: Human osteoarthritis and an experimental model of joint degeneration. *Osteoarthritis and Cartilage*, **7**, 2-14.

Shepherd, D.E.T., & Seedhom B.B. (1997). A technique for measuring the compressive modulus of articular cartilage under physiological loading rates with preliminary results. *Journal of Engineering in Medicine*, **211**, 155-165.

Stolk, J., Verdonschot, N., Cristofolini, L., Toni, A., & Huiskes, R. (2002). Finite element and experimental models of cemented hip joint reconstructions can produce similar bone and cement strains in pre-clinical tests. *Journal of Biomechanics*, **35**, 499-510.

Wu, J.Z., Herzog, W., & Epstein, M. (1998). Effects of inserting a pressensor film into articular joints on the actual contact mechanics. *Journal of Biomechanical Engineering*, **120**, 655-659.